Charge-Transfer Processes in Warm Dense Matter: Selective Spectral Filtering for Laser-Accelerated Ion Beams

J. Braenzel,[1] M. D. Barriga-Carrasco,[2] R. Morales,[2] and M. Schnürer[1]
[1]*Max Born Institute, Max Born Straße 2a, D-12489 Berlin, Germany*
[2]*E.T.S.I. Industriales, Universidad de Castilla-La Mancha, E-13071 Ciudad Real, Spain*

(Received 1 December 2017; published 4 May 2018)

We investigate, both experimentally and theoretically, how the spectral distribution of laser accelerated carbon ions can be filtered by charge exchange processes in a double foil target setup. Carbon ions at multiple charge states with an initially wide kinetic energy spectrum, from 0.1 to 18 MeV, were detected with a remarkably narrow spectral bandwidth after they had passed through an ultrathin and partially ionized foil. With our theoretical calculations, we demonstrate that this process is a consequence of the evolution of the carbon ion charge states in the second foil. We calculated the resulting spectral distribution separately for each ion species by solving the rate equations for electron loss and capture processes within a collisional radiative model. We determine how the efficiency of charge transfer processes can be manipulated by controlling the ionization degree of the transfer matter.

DOI: 10.1103/PhysRevLett.120.184801

Ion projectiles traveling through solid, cold matter reach an equilibrium charge state achieved after a short distance. The projectiles charge states are mainly a function of its velocity. The evolution of charge states for ions moving in ionized, warm dense matter (WDM) and with it the energy loss remains an unsolved fundamental problem [1–6]. Since the energy loss of ions in matter scales approximately proportional to the square of its charge state, a predictability of the charge states is essential for the nuclear fusion processes, e.g., the impact of ion heating or, in general, the investigation of laser induced fusion [7–11]. Moreover, the underlying cross sections and dynamics are bound to fundamental astrophysical questions that relate on high density warm and hot dense matter [12–14]. The study of ion charge transfer processes and energy loss in heated matter has important applications, as, e.g., pulsed ion sources for medical applications [15–18] and plasma stripper foils for the ion acceleration technology [19,20]. Up to now, there exist only few experimental data in order to verify different theoretical predictions and a wide range of parameters [21–26], which is insufficient for the validation. Presently, a large number of experiments are in preparation that investigate the interaction of ion beams with laser ionized matter [10,11,27], as the laser illumination enables an ionization and heating of a transfer matter even at a high density. Laser accelerated ion beam sources were proposed to provide a compact experimental setup in which the charge evolution in the needed parametric range can be investigated: it can deliver moderate to high ion velocities, high particle numbers, a short ion pulse duration, and low emittance [26,28–32]. The present research on laser ion acceleration itself searches for a compact solution that could narrow the spectral bandwidth, a necessary prerequisite for its possible future applications [17,33–35]. In this Letter, we investigate experimentally and theoretically the interaction of a laser accelerated carbon ion beam, with an ionized ultrathin foil and show how this affects the final charge distribution. For the ion pulse, a second transfer foil acts like a charge depending spectral filter, as the underlying processes scale with the velocity and charge state. Our findings show that this WDM filtering process led for some charge states to a significant reduction of their spectral bandwidth. We explain the experimental findings by numerical calculations of the rate equations using the cross-section model of Ref. [2]. We show that our calculations reproduce each particle distribution in good agreement when a partial ionization of the transfer foil is taken into account. With this, we introduce a novel and very compact method for spectral shaping of laser generated ion beams that can directly manipulate its impact on a particular spectral range by the ionization of the transfer foil.

In the relativistic laser plasma acceleration schemes, like TNSA (target normal sheath acceleration) and radiation pressure acceleration [28,36], usually the resulting ion beam spans a broad range of kinetic energies (0.1–100 MeV) and multiple charge states [32,37]. The accelerated ion bunch is always accompanied by an emission of extreme ultraviolet (XUV) radiation, transmitted laser light [38,39], and a comoving, diverging electron sheath [28,40]. This makes it possible to ionize and heat a close to the target placed foil shortly before the ion beam arrives. Such a setup provides a compact, built-in plasma stripper foil. We realized this experimental condition with a double foil target that consists of two ultrathin polymer foils with a separation distance of about 500 μm. Our laser ion

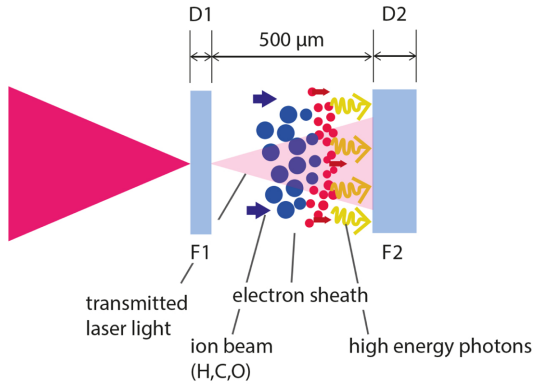

FIG. 1. Scheme of the experimental setup with a double foil target. The first foil serves as target ($F1$) and the second foil ($F2$) as transfer matter. The separation distance between the foils is about 500 μm and allows a partial ionization of the second foil due to transmitted laser light, emitted high energy photons, and the expanding electron sheath.

acceleration experiments were performed at the former high field laser of the Max Born Institute. The system was a Ti: sapphire laser system with a pulse duration of 35 fs and $\lambda_L = 800$ nm, at ultrahigh laser contrast (prepulse free, ASE to peak level 10^{14} in a few ps time scale by the use of a double plasma mirror [32,41]). The laser pulse reached an averaged intensity of 5×10^{19} W/cm^2 FWHM of the focal area, which was about 4 μm in diameter. The double foil target system consisted of two steel hole plates on which ultrathin polymer foils, poly-vinyl-formal ($C_5H_7O_2$, 1.23 g/cm^3), were attached [42]. This target system enabled freestanding foils on a diameter of 600 μm that were separated by about 500 μm due to the target holder construction. The laser interacted with the first foil ($F1$) at normal incidence. The ions were detected in the laser propagation direction by a Thomson spectrometer (static magnet and an applied high static electric field) and a Hamamatsu microchannel plate as detector, with a 100 mm diameter. The detector was calibrated concerning the particle sensitivity with the help of alpha particles emitted from an Am204 source [43]. A schematic of the setup is depicted in Fig. 1. Partly the second foil $F2$ was removed to measure a reference ion distribution from a single foil configuration.

In Fig. 2, the ion raw spectra obtained by a single foil with a thickness $D(F1) = 14$ nm is compared to the spectra obtained in the presence of a $D(F2) = 35$ nm transfer foil. According to their thickness and density, the energy loss of ions in $F2$ is very small and is neglected in the following.

The carbon ion spectra we obtained from the single foil configuration are distributed over a broad kinetic energy (0.1–18 MeV) range. In such a single foil configuration, the dominant carbon species with the highest kinetic energy and highest overall particle number is C^{6+}. It is followed by C^{5+}, C^{4+}, and then C^{3+}, which is already close to the

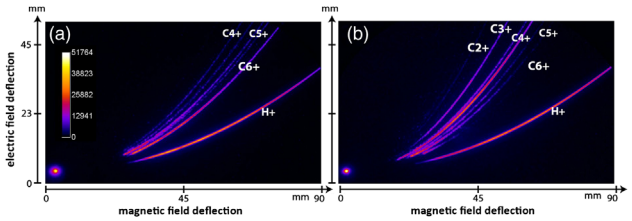

FIG. 2. Change in the ion particle numbers per charge state versus velocity by using a two foil target setup with first foil $F1$ at thickness 14 nm and second foil $F2$ at 35 nm. Detector image of the ions after having passed a Thomson spectrometer (a) from single foil configuration and (b) from double foil configuration, both in the same color scaling.

detector threshold value. In the presence of the second foil, a significant change in the spectral distribution of each charge species becomes apparent: while the overall particle number remains constant within 5%, the particle number of each charge state does not (cf. Fig. 2). Here, a significant redistribution of the particle number for each charge state in dependency on their velocity is observed. Figure 3 demonstrates the relative change of the particle number of each carbon ion as a function of the kinetic energy between the double and single foil targets. Clearly, one can see that up to a particular velocity the particle number of the highest carbon charge states declines in the same way as it raises for the lower charge states. As a consequence, the energy distribution of C^{6+} and C^{5+} ions is detected with a narrowed spectral bandwidth at the high kinetic energy range of about $\Delta E_{\mathrm{FWHM}}/E(C^{6+}) = 0.35$ at 12 MeV and $\Delta E_{\mathrm{FWHM}}/E(C^{5+}) = 0.67$ at 7 MeV (cf. Figs. 2 and 4 for the corresponding evaluated spectral distribution). For the here considered ion kinetic energies, electron capture and loss processes in the second foil affect the spectral distribution of the carbon ions similar to a charge and velocity dependent filtering process. This remarkably reduces their spectral bandwidth.

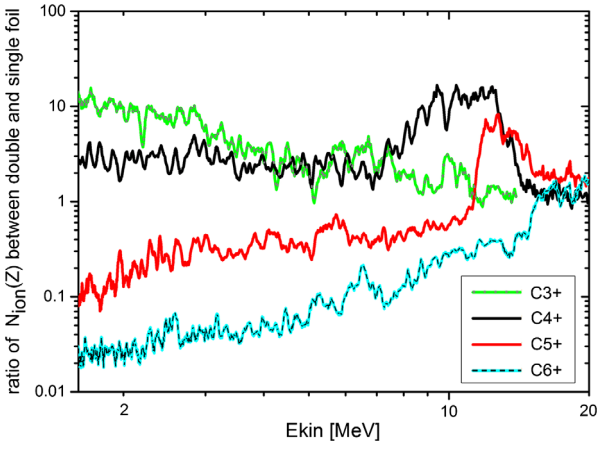

FIG. 3. Ratio of particle numbers $N_{\mathrm{ion}}(Z)$ between double and single foil measurements $[N_{\mathrm{ion}}\ (F1F2)/N_{\mathrm{ion}}\ (F1)]$ (cf. Fig. 3) for each carbon charge state as a function of their kinetic energy.

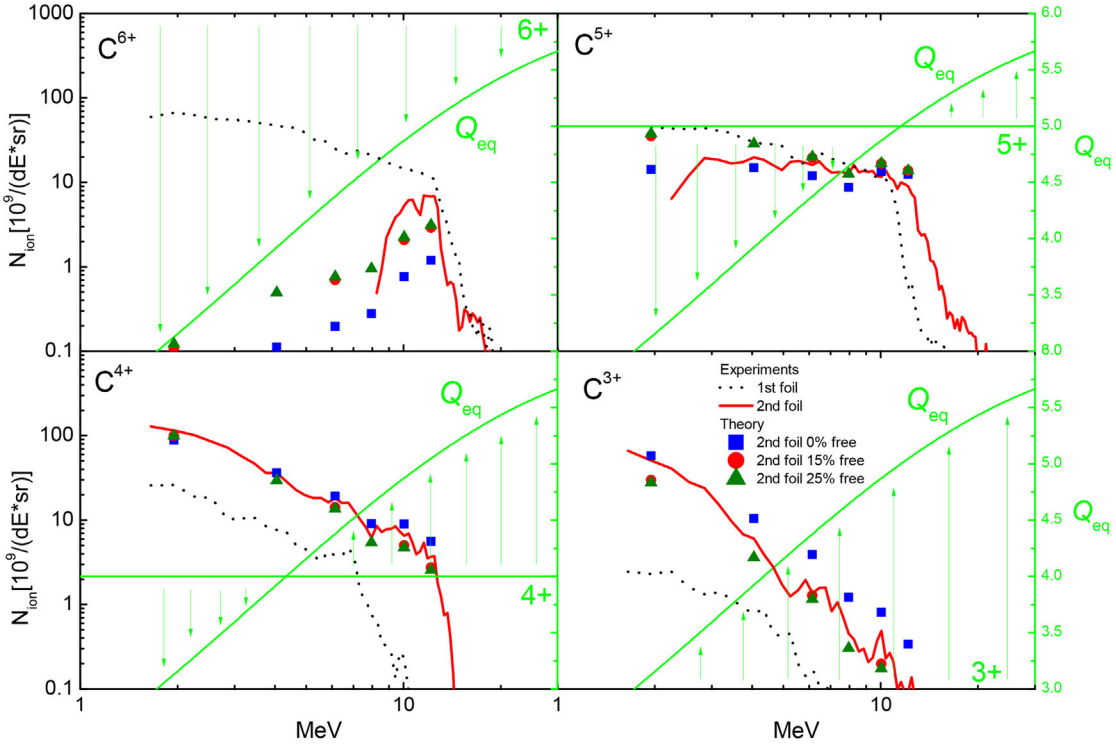

FIG. 4. Evaluated kinetic energy spectrum of each charge state for the ion beam of Fig. 2. The spectral distribution detected from the single foil setup (black dotted line) is compared to the one from the double foil interaction (straight red line). The initial ion beam spectral distribution and foil parameters were used for calculating the charge transfer for each single carbon charge state when passed through a transfer foil according to (2). Blue squares give the result from a nonionized transfer matter, red dots from the calculation assuming a 15% ionization, and green triangles for a 25% one.

When the ion beam travels through a transfer matter, its charge state is determined by a dynamical equilibrium established by charge exchange processes, namely, the electron loss and capture processes. In general, these are determined by the particular cross sections, which are themselves a function of the projectiles velocity v, the atomic number A, plasma temperature T, density n_e, and ionization degree Z_i.

The charge state distribution of the ion beam F_q, normalized according to $\sum_{q=0}^{Z_{\max}} F_q(t) = 1$, can be obtained by solving the rate equations

$$\frac{dF_q(t)}{dt} = C_{q+1}F_{q+1}(t) + L_{q-1}F_{q-1}(t) - (C_q + L_q)F_q(t), \tag{1}$$

where C_q and L_q are the ratios of the projectile electron capture and loss, describing the number of transitions from the charge state q to the charge state q' per unit time. Further details about (1) can be found in [4]. The C_q and L_q ratios used in our study based on the work by Peter and Meyer-ter-Vehn [2] take into account the cross sections for the projectile ionization by Coulomb collisions with the target ions or target free electrons and for the projectile recombination by radiative electron capture, three-body recombination, dielectronic recombination, and bound electrons capture.

The mean charge state of the ion beam is given by

$$Q(t) = \sum_{q=0}^{Z} qF_q(t). \tag{2}$$

In the stationary case $dF_q(t)/dt = 0$, the model for a resulting mean charge is usually simplified by the description of an equilibrium charge state $Q(t_{\mathrm{eq}}) = Q_{\mathrm{eq}}$ [3,4]. The equilibrium state provides a good approximation for the projectile charge for a sufficient long traveling length in the transfer matter. If this is not fulfilled, we have to consider that the ions have a different, instantaneous charge during their traveling through the transfer matter, just before reaching the equilibrium [4].

Taken into account the complex situation of the multispecies charge and energy distribution our experiment provides, we calculated the charge state distribution as a function of projectiles kinetic energy for the particle numbers of each carbon species for C^{3+}, C^{4+}, C^{5+}, and C^{6+} using Eq. (1). For this calculation, we used for the initial distribution the experimentally obtained one (cf. Figs. 2 and 4) and implemented the same foil parameter as in the experiment with and without partially ionization.

The results of our calculations are shown in Fig. 4 and compares the ion charge and kinetic energy distribution without the second foil, with the one that passed through the transfer foil, respectively. The comparison reveals how the ionization of the transfer foil affects the efficiency of charge exchange processes. The overlay in Fig. 4 highlights the connection between each single carbon ion spectrum and the equilibrium charge Q_{eq}.

Apparently, the particle numbers of the lower charge state (C^{3+}) are raised about one order of magnitude over the whole spectral range. This leads to a higher cutoff energy and has to be attributed to the electron capture processes of ions with a higher charge state. Here, Q_{eq} is higher than 3+ in most of the energy range and indicates a strong tendency for ionization of C^{3+} that would lead to a decrease of the particle number. The particle numbers of C^{3+} are comparatively small, and this explains why the higher charge states predominate over its ionization processes. The case is similar for C^{4+}: the particle number raises in the whole energy range due to the electron capture of higher charge states of C^{5+} and C^{6+} or the electron loss of C^{3+}. The sum of all these latter processes from the higher and lower charge states raise the particle number of C^{4+} and exceed the ion numbers of the capture and loss processes for C^{4+}.

For C^{5+}, the particle number declines < 8 MeV due to electron capture processes in the second foil. This corresponds to Q_{eq} which lies below 5+ in this energy range. For higher energies > 10 MeV, the number of C^{5+} particles increase, as Q_{eq} reaches values $> 5+$. Similar to lower charge states, the maximum kinetic energy of C^{5+} reaches higher values by passing through the transfer foil. This effect can only result from the electron capture processes of the C^{6+} ions, which solely reached such high kinetic energies. Finally, concerning C^{6+}, for the lower kinetic energy range, the equilibrium charge is far below 6+ leading to efficient electron capture processes and enabling the strong suppression of the low energetic spectrum. For energies > 12 MeV, the C^{6+} particle distribution remains more or less the same as in the case of the distribution obtained from the one single foil measurement, because here Q_{eq} is close to the value of 6+.

In Fig. 3 and the comparison of the resulting spectral distributions with Q_{eq} in Fig. 4, it becomes clear that the model of Q_{eq} cannot be easily transferred to an ion bunch consisting of different charge states. Moreover, with the ionization degree of the second foil, one can manipulate the resulting charge and with it spectral distribution of a particular charge state.

Because of the dependency of the rate equations (cross sections) on the ion charge state and velocity, the impact of charge exchange processes is very different for each charge state in the discussed kinetic energy range. Moreover, with ionizing the transfer foil, the efficiency of electron capture processes is decreased for the highest charge states. In consequence, a higher ionization degree of the transfer foil leads to corresponding lower particle numbers for the lower charge states (C^{4+} and C^{3+}). Our measurements and theoretical calculation extend the former investigation of Ref. [26] with an ion beam distribution that provided fully ionized carbon as the dominant species and a higher kinetic energy range. For kinetic energies below 7 MeV, the electron capture processes dominate the highly charged carbon ions, while the electron loss processes set in for higher kinetic energies. The contribution of electron loss processes from lower charge states is small, which can be explained by their comparable small particle number. Our theoretical calculations demonstrated how the efficiency of the charge exchange processes can be manipulated by the degree of ionization of the transfer matter. A higher degree of ionization for the second foil delivers a better agreement with our experimental data. Such an ionization is reasonable for our experimental setup. It can be caused by a few percent of laser light leaking through the first foil [38,39], emitted XUV radiation, and by the electron sheath (few keV) foil that accompanies the ions in the late TNSA stage. Our findings showed that charge transfer processes in the ionized transfer foil have different impacts on the spectral distribution of each charge state. For complex charge and spectral distributions, as found in our experiments, viewing each single charge state reveals a detailed insight and prediction in comparison to a summarized picture of Q_{eq}. In view of the acceleration mechanisms of multi-ion species by a laser and ultrathin foil interaction, here the question arises of how the acceleration itself could be influenced by charge transfer processes inside the plasma.

In conclusion, we have presented experimental data for charge transfer processes in a wide kinetic energy range (0.1–18 MeV) for a laser accelerated carbon ion beam with a thin and partially ionized transfer matter. Our experiments showed that for some charge states of the ion beam the charge transfer processes act like a velocity dependent charge selective filtering process. In the kinetic energy range (0.1–0.6 MeV/u), electron capture processes are dominant. This redistributes the ions towards lower charge states. For higher kinetic energies, electron loss processes become dominant. As a consequence, this filters the spectral distribution of the highest charge states of carbon and results in a remarkable narrow spectral bandwidth in the high kinetic energy range. The complex evolution of carbon ion charge states in the transfer matter we calculated for the ion beam distribution from the single foil measurement. We used a collisional-radiative model and solved the rate equations. Our calculations reproduced the resulting spectral distribution of each single charge state in good agreement for a partially ionized and ultrathin transfer matter. The efficiency of the charge exchange can be altered by a partial ionization of the transfer foil, and this affects the ion distribution for each charge state. Ionization of the

transfer foil can be used in order to manipulate the resulting ion distribution of a single charge state. The used double foil target system provides for the laser ion acceleration a built-in plasma stripper foil device, which benefits from ionization by the help of the transmitted laser light, emitted XUV light, and electrons from the target. Either by different separation distances or by an additional preheating of the second foil at its backside with a second strong laser pulse, the ionization and plasma temperature of the second foil can be easily accessed. A detailed parametric examination of the ion beam and transfer foil (mass number, energy and charge distribution, foil separation distance, ionization degree) remains as promising objectives for future investigations.

This project has received funding from the European Union's Horizon 2020 research and innovation programme under grant agreement No. 654148 Laserlab-Europe and by the Deutsche Forschungsgemeinschaft CRC/Transregio 18. Also, this research was funded by UCLM Ayuda Interna a Grupos de Investigacin 01110G7041. R. M. wants to thank CATEDRA ENRESA-UCLM for Grant No. 2017-BCL-6415. We thank D. Sommer for his excellent work on the target foil production and L. Ehrentraut for the laser operation.

[1] S. Kreussler, C. Varelas, and W. Brandt, Phys. Rev. B **23**, 82 (1981).
[2] T. Peter and J. Meyer-ter-Vehn, Phys. Rev. A **43**, 2015 (1991).
[3] M. D. Barriga-Carrasco, D. Casas, and R. Morales, Phys. Rev. E **93**, 033204 (2016).
[4] R. Morales, M. D. Barriga-Carrasco, and D. Casas, Phys. Plasmas **24**, 042703 (2017).
[5] M. Roth, C. Stckl, W. Süss, O. Iwase, D. O. Gericke, R. Bock, D. H. H. Hoffmann, M. Geissel, and W. Seelig, Europhys. Lett. **50**, 28 (2000).
[6] G. Xu *et al.*, Phys. Rev. Lett. **119**, 204801 (2017).
[7] W. Cayzac *et al.*, Nat. Commun. **8**, 15693 (2017).
[8] B. B. Back, H. Esbensen, C. L. Jiang, and K. E. Rehm, Rev. Mod. Phys. **86**, 317 (2014).
[9] G. Faussurier, C. Blancard, and M. Gauthier, Phys. Plasmas **20**, 012705 (2013).
[10] A. Levy *et al.*, Phys. Plasmas **22**, 030703 (2015).
[11] M. Nakatsutsumi, K. Appel, C. Baehtz, B. Chen, T. E. Cowan, S. Göde, Z. Konopkova, A. Pelka, G. Priebe, A. Schmidt, K. Sukharnikov, I. Thorpe, T. Tschentscher, and U. Zastrau, Plasma Phys. Controlled Fusion **59**, 014028 (2017).
[12] B. Friedman and G. DuCharme, J. Phys. B **50**, 115202 (2017).
[13] N. Booth, A. P. L. Robinson, P. Hakel, R. J. Clarke, R. J. Dance, D. Doria, L. A. Gizzi, G. Gregori, P. Koester, L. Labate, T. Levato, B. Li, M. Makita, R. C. Mancini, J. Pasley, P. P. Rajeev, D. Riley, E. Wagenaars, J. N. Waugh, and N. C. Woolsey, Nat. Commun. **6**, 8742 (2015).
[14] B. A. Remington, D. Arnett, R. Paul, Drake, and H. Takabe, Science **284**, 1488 (1999).
[15] E. Stoffels, I. E. Kieft, R. E. J. Sladek, L. J. M. van den Bedem, E. P. van der Laan, and M. Steinbuch, Plasma Sources Sci. Technol. **15**, S169 (2006).
[16] P. Mur, P. Bellido, M. Seimetz, R. Lera, A. R. de la Cruz, M. Galan, L. Roso, F. Sanchez, and J. Benlloch, J. Instrum. **12**, C03083 (2017).
[17] U. Masood, T. E. Cowan, W. Enghardt, K. M. Hofmann, L. Karsch, F. Kroll, U. Schramm, J. J. Wilkens, and J. Pawelke, Phys. Med. Biol. **62**, 5531 (2017).
[18] L. Karsch, E. Beyreuther, W. Enghardt, M. Gotz, U. Masood, U. Schramm, K. Zeil, and J. Pawelke, Acta Oncologica **56**, 1359 (2017).
[19] M. Chabot, D. Gardès, P. Box, J. Kiener, C. Deutsch, G. Maynard, V. André, C. Fleurier, D. Hong, and K. Wohrer, Phys. Rev. E **51**, 3504 (1995).
[20] Y. Oguri, K. Tsubuke, A. Sakumi, K. Shibata, R. Sato, K. Nishigori, J. Hasegawa, and M. Ogawa, Nucl. Instrum. Methods Phys. Res., Sect. B **161–163**, 155 (2000).
[21] J. A. Frenje, P. E. Grabowski, C. K. Li, F. H. Séguin, A. B. Zylstra, M. Gatu Johnson, R. D. Petrasso, V. Y. Glebov, and T. C. Sangster, Phys. Rev. Lett. **115**, 205001 (2015).
[22] E. Nardi and Z. Zinamon, Phys. Rev. Lett. **49**, 1251 (1982).
[23] C. Deutsch and G. Maynard, Phys. Rev. A **40**, 3209 (1989).
[24] K. G. Dietrich, D. H. H. Hoffmann, E. Boggasch, J. Jacoby, H. Wahl, M. Elfers, C. R. Haas, V. P. Dubenkov, and A. A. Golubev, Phys. Rev. Lett. **69**, 3623 (1992).
[25] J. Jacoby, D. H. H. Hoffmann, W. Laux, R. W. Muller, H. Wahl, K. Weyrich, E. Boggasch, B. Heimrich, C. Stockl, H. Wetzler, and S. Miyamoto, Phys. Rev. Lett. **74**, 1550 (1995).
[26] M. Gauthier *et al.*, Phys. Rev. Lett. **110**, 135003 (2013).
[27] G. A. Mourou, G. Korn, W. Sandner, and J. L. Collier, *Extreme Light Infrastructure, White Book, Science and Technology with Ultra-Intense Lasers* (THOSS Media GmbH, Berlin, 2015).
[28] H. Daido, M. Nishiuchi, and A. S. Pirozhkov, Rep. Prog. Phys. **75**, 056401 (2012).
[29] A. Macchi, A. Sgattoni, S. Sinigardi, M. Borghesi, and M. Passoni, Plasma Phys. Controlled Fusion **55**, 124020 (2013).
[30] F. Mollica, L. Antonelli, A. Flacco, J. Braenzel, B. Vauzour, G. Folpini, G. Birindelli, M. Schnürer, D. Batani, and V. Malka, Plasma Phys. Controlled Fusion **58**, 034016 (2016).
[31] S. Ter-Avetisyan, J. Braenzel, M. Schnürer, R. Prasad, M. Borghesi, S. Jequier, and V. Tikhonchuk, Rev. Sci. Instrum. **87**, 02B134 (2016).
[32] J. Braenzel, A. A. Andreev, K. Platonov, M. Klingsporn, L. Ehrentraut, W. Sandner, and M. Schnürer, Phys. Rev. Lett. **114**, 124801 (2015).
[33] A. Macchi, A. Sgattoni, S. Sinigardi, M. Borghesi, and M. Passoni, Plasma Phys. Controlled Fusion **55**, 124020 (2013).
[34] L. Pommarel, B. Vauzour, F. Mégnin-Chanet, E. Bayart, O. Delmas, F. Goudjil, C. Nauraye, V. Letellier, F. Pouzoulet, F. Schillaci, F. Romano, V. Scuderi, G. A. P. Cirrone, E. Deutsch, A. Flacco, and V. Malka, Phys. Rev. Accel. Beams **20**, 032801 (2017).
[35] A. Russo *et al.*, J. Instrum. **12**, C01031 (2017).
[36] T. Esirkepov, M. Yamagiwa, and T. Tajima, Phys. Rev. Lett. **96**, 105001 (2006).

[37] A. Henig, S. Steinke, M. Schnürer, T. Sokollik, R. Hörlein, D. Kiefer, D. Jung, J. Schreiber, B. M. Hegelich, X. Q. Yan, J. Meyer-ter Vehn, T. Tajima, P. V. Nickles, W. Sandner, and D. Habs, Phys. Rev. Lett. **103**, 245003 (2009).

[38] J. Braenzel, A. A. Andreev, F. Abicht, L. Ehrentraut, K. Platonov, and M. Schnürer, Phys. Rev. Lett. **118**, 014801 (2017).

[39] V. Bagnoud, J. Hornung, T. Schlegel, B. Zielbauer, C. Brabetz, M. Roth, P. Hilz, M. Haug, J. Schreiber, and F. Wagner, Phys. Rev. Lett. **118**, 255003 (2017).

[40] T. Esirkepov, M. Yamagiwa, and T. Tajima, Phys. Rev. Lett. **96**, 105001 (2006).

[41] M. P. Kalashnikov, H. Schönnagel, and W. Sandner, AIP Conf. Proc. **1465**, 13 (2012).

[42] J. Braenzel, C. Pratsch, P. Hilz, C. Kreuzer, M. Schnürer, H. Stiel, and W. Sandner, Rev. Sci. Instrum. **84**, 056109 (2013).

[43] R. Prasad, M. Borghesi, F. Abicht, P. V. Nickles, H. Stiel, M. Schnürer, and S. Ter-Avetisyan, Rev. Sci. Instrum. **83**, 083301 (2012).